Pergamon

Geochimica et Cosmochimica Acta, Vol. 66, No. 22, pp. 3913–3926, 2002

0016-7037/02 $22.00 + .00

PII S0016-7037(02)00966-3

The effect of pH and temperature on kaolinite dissolution rate under acidic conditions

JORDI CAMA,[1] VOLKER METZ,[2] and JIWCHAR GANOR*

Department of Geological and Environmental Sciences, Ben-Gurion University of the Negev, P. O. Box 653, Beer-Sheva 84105, Israel.

(*Received August* 17, 2001; *accepted in revised form May* 6, 2002)

Abstract—The main goal of this paper is to demonstrate a new rate law describing the combined effect of pH (0.5 to 4.5) and temperature (25°C to 70°C) on kaolinite dissolution rate, under far from equilibrium conditions, as a step towards establishing the full rate law of kaolinite dissolution under acidic conditions. Dissolution experiments were carried out using non-stirred flow-through reactors fully immersed in a thermostatic water bath held at a constant temperature of 25.0°C, 50.0°C or 70.0°C ± 0.1°C. Kaolinite dissolution rates were obtained based on the release of silicon and aluminum at steady state. The results show good agreement between these two estimates of kaolinite dissolution rate. Kaolinite dissolution rates range as a function of temperature and fluid composition from $8 \pm 1 \times 10^{-15}$ mol m^{-2} s^{-1} (at 25°C and pH 4.5) to $1.5 \pm 0.2 \times 10^{-11}$ mol m^{-2} s^{-1} (at 70°C and pH 0.5). In general, dissolution rate increases with temperature and decreases with pH.

The combined effect of pH and temperature is modeled by two independent proton promoted reaction paths. The first reaction path controls the overall dissolution rate at pH ≥ 2.5, whereas the second path controls it below pH 0.5. Between pH 0.5 and 2.5 the two reaction paths influence the rate. Using this model the effects of pH and temperature on the overall dissolution rate of kaolinite under acidic condition can be described by:

$$Rate = 2 \cdot 10^{2} \cdot e^{-22/RT} \cdot \frac{2 \cdot 10^{-10} \cdot e^{19/RT} \cdot a_{H^+}}{1 + 2 \cdot 10^{-10} \cdot e^{19/RT} \cdot a_{H^+}} + 5 \cdot 10^{7} \cdot e^{-28/RT} \cdot \frac{1.4 \cdot 10^{-7} \cdot e^{10/RT} \cdot a_{H^+}}{1 + 1.4 \cdot 10^{-7} \cdot e^{10/RT} \cdot a_{H^+}}$$

where R is the gas constant, T is the temperature (K) and a_{H^+} is the activity of protons in solution.

1. INTRODUCTION

The most studied aspect of weathering of aluminosilicates in general and kaolinite in particular has been the dependence of dissolution rates on pH. Metz and Ganor (2001) compare the results of kaolinite dissolution rates at 25°C and pH 3 as obtained in their study, with those of Carroll-Webb and Walther (1988), Wieland and Stumm (1992) and Ganor et al. (1995). The dissolution rates obtained by Ganor et al. (1995) agree with those of Wieland and Stumm (1992) and are four to five times faster than the rates obtained by Carroll-Webb and Walther (1988). Metz and Ganor (2001) suggested that differences in kaolinite dissolution rates observed by the different studies are a result of differences in stirring efficiency. They showed that although kaolinite dissolution at low temperature is surface-controlled and not diffusion-controlled, calculated dissolution rate is enhanced by stirring. Since the stirring effect on kaolinite dissolution rate varies with temperature and pH, measurement of kinetic parameters such as activation energy may be influenced by stirring. As a result, kinetic factors obtained under non-stirred conditions were suggested to be better approximations for the real kinetic factors, at least for slow reactions that are not influenced by diffusion, such as kaolinite dissolution (Ganor and Metz, 2001). Therefore, a new data set examining the effect of both temperature and pH on dissolution rate under non-stirred conditions is required.

In the absence of catalysts, the dissolution rate of oxides and silicates was classically interpreted by three reaction mechanisms: proton promoted, hydroxyl promoted and water-promoted, that dominate the reaction rate under acidic, alkaline or near neutral conditions, respectively. As the proton promoted mechanism dominated the dissolution rate under acidic conditions, it was shown for many minerals that the dissolution rate, within certain pH ranges, is proportional to a fractional power of the hydrogen ion activity:

$$Rate = k_{H^+} \cdot a_{H^+}^{n_{H^+}} \tag{1}$$

where a^{H^+} is the activity of protons in the solution, n_{H^+} is the order of the reaction with respect to H^+ and k_{H^+} is a rate coefficient. Silicate dissolution is a surface process and therefore, it is more appropriate to express the dependence of the rate on the concentration (or activity) of protons adsorbed on the surface rather than on the bulk activities in solution. Hence, Eqn. 1 can be written in terms of surface concentrations ($X_{i,ads}$):

$$Rate = k'_{H^+} \cdot X_{H^+,ads}^{n_{H^+,ads}} \tag{2}$$

Eqns. 1 and (2) describe the pH effect on dissolution rate under conditions in which a **single mechanism** is dominant throughout all experiments. One of the goals of the present study is to show that two mechanisms control the rate in the pH range of 0.5 to 4.5.

Fig. 1 compares kaolinite dissolution rates at 25°C and 80°C

* Author to whom correspondence should be addressed (ganor@bgumail.bgu.ac.il).
[1] *Present address:* Department of Environmental Geology, Institute of Earth Sciences "Jaume Almera," CSIC, Lluís Solé i Sabarís s/n, Barcelona 08028, Catalonia (Spain).
[2] *Present address:* Institut für Nukleare Entsorgung, Forschungszentrum Karlsruhe (FZK-INE), P. O. Box 3640, Karlsruhe 76021, Germany.

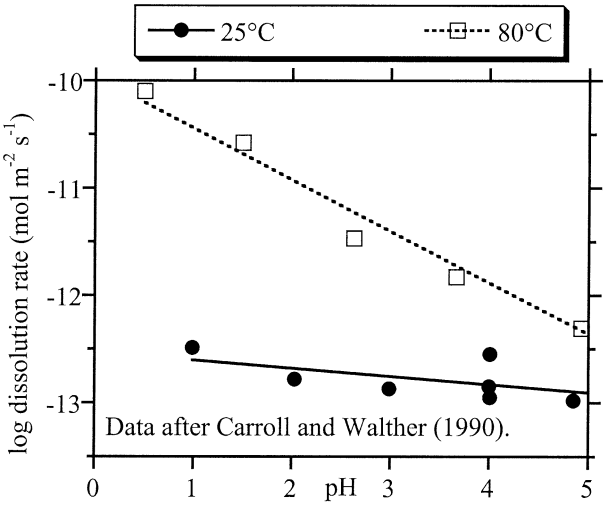

Fig. 1. Comparison of the effect of pH on kaolinite dissolution rate at 25°C to that at 80°C. Source data: Carroll and Walther (1990).

as obtained by Carroll and Walther (1990). Calculating the reaction order from the slopes of the lines in Fig. 1 shows that the reaction orders with respect to a_{H^+} increase with temperature from 0.08 ± 0.03 (R^2 = 0.52) at 25°C to 0.48 ± 0.03 (R^2 = 0.98) at 80°C.

Carroll and Walther (1990) calculated activation energies for kaolinite dissolution based on their experiments. They recalculated the dissolution rates at each pH at 25°C and 80°C from the reaction orders that were derived using Eqn. 1 from the experiments. As a result of the significant difference between the reaction order at 25°C and at 80°C (Fig. 1), calculated values of activation energy range from 1.7 kcal/mol at pH 7 to 16 kcal/mol at pH 1.

There are two hidden assumptions in using Eqn. 1 for modeling a surface reaction: (1) the reactive surfaces do not become saturated with respect to protons as the pH decreases; and (2) only one mechanism dominates the rate throughout the examined pH (and temperature) range. Both assumptions were challenged in previous studies. Wieland and Stumm (1992) proposed that the overall dissolution rate of kaolinite at 25°C under acidic conditions could be explained by two independent parallel dissolution reactions, one at the edge and the other at the gibbsite layer. They observed a constant dissolution rate in the pH range of 2 to 3 and explained it by saturation of the gibbsite layer with protons. Similarly, surface saturation was suggested by Ganor et al. (1995) as an explanation for their observation that kaolinite dissolution rate at 50°C is about constant below pH 3. Recently, Huertas et al. (1999) re-determined the effect of pH on kaolinite dissolution rate and presented a surface coordination model that confirms that the mechanism of kaolinite dissolution under acidic conditions is controlled by two distinct surface complexes. If, as was suggested by previous studies, kaolinite surfaces show saturation with respect to H^+ and kaolinite dissolution rate under acidic conditions is dominated by more than one mechanism, then previously obtained pH dependencies and apparent activation energies that were calculated based on Eqn. 1 cannot contribute to the understanding of the dissolution mechanism.

Saturation of reactive surfaces with respect to protons and changes in reaction mechanism may be detected by changes in the slope of a log rate vs. pH plot. To be able to accurately model the information in such a plot it is important to conduct a dense array of experiments, as was done in the present study.

Oelkers et al. (1994) and Devidal et al. (1997) show that aluminum inhibits kaolinite dissolution even under very far from equilibrium conditions. As aluminum concentrations varied in experiments conducted under different experimental conditions, it is important to examine the aluminum effect on rate to distinguish it from other effects such as temperature and pH.

In the present study we introduce a new data set examining the effect of both temperature (25°C to 70°C) and pH (0.5 to 4.5) under non-stirred conditions on kaolinite dissolution rate. The effects of other variables such as aluminum concentration and ionic strength on rate are examined as well as their possible effects on pH and temperature dependencies on dissolution rate. The main objective of the paper is to model the experimental data using two reaction mechanisms, and to obtain a new rate law describing the effect of pH and temperature.

2. MATERIALS AND METHODS

2.1. Characterization and Pretreatment of kaolinite

The kaolinite sample used in this study is the KGa-2 (Warren county, Georgia), an international reference sample of the Clay Mineral Society Source Clay Repository that was supplied by the Yale Peabody Museum. Sample KGa-2 is an almost pure kaolinite, containing more than 96 wt.% of $Al_2Si_2O_5(OH)_4$. Major impurities are TiO_2 and Fe_2O_3. The kaolinite was pretreated in 0.001 N $HClO_4$ at 80°C for few months, using the procedure described in Ganor et al. (1995). Surface area was measured using a Micromeritics Gemini 2370 surface area analyzer. The BET-determined initial surface area of the kaolinite was 18.5 ± 10% $m^2\ g^{-1}$ using 5-point N_2 adsorption isotherms. Usually, the surface area after each experiment was (within error) the same as the initial area (Table 1).

2.2.. Experimental Setting

Dissolution experiments were carried out using non-stirred flow-through reactors (ca. 35 mL in volume) fully immersed in a thermostatic water-bath held at a constant temperature of 25.0°C, 50.0°C or 70.0°C ± 0.1°C. The reaction cells were composed of two chambers, a lower chamber of 33-mm inner diameter and an upper chamber of 26-mm inner diameter. The two chambers were separated by a fine (5 μm) nylon mesh, on which kaolinite powder was placed. A schematic sketch of the experimental setting and some more details of the experimental procedure can be found in Metz and Ganor (2001). Most of the experiments lasted longer than 1500 h, and consisted of a single stage, i.e., the experiment was stopped after steady state was attained. A few experiments consisted of two or more stages, in each of which Al or Si input concentrations and/or the flow rate were changed. Calculated total dissolved material throughout the experiments was less than 5% of the starting mass of kaolinite.

Input solutions were prepared at specific pH and with specific concentrations of total Si and Al by mixing $HClO_4$ (70%, BDH) source solution, variable amounts of aluminum and silicon source solutions and double deionized water. The silicon source solution was a dissolved $Na_2H_2SiO_4{\cdot}5H_2O$, (1000 ppm, BDH) and the aluminum source solution was $AlCl_3$ standard solution (1000 ppm, Merck). In several cases, adequate quantities of 0.25 mol/L NaOH solution were added into the input solution to obtain the desired output pH. In experiments designed to study the effect of ionic strength, different amounts of $NaClO_4$ have been added into the input solution.

Input and output solutions were analyzed for Al, Si, and pH. Total Al and Si were analyzed colorimetrically with a UV-visible spectrophotometer, using the Catechol violet method (Dougan and Wilson, 1974) and Molybdate blue method (Koroleff, 1976), respectively. Before

Table 1. Experimental conditions and results.

Experiment	Duration (h)	Flow rate (mL min^{-1})	pH input	pH output	Al input (μM)	Al output (μM)	Si input (μM)	Si output (μM)	$SR_{Al/Si}$	final mass (g)	BET area (m^2g^{-1})	$Rate_{Al}$ (mol m^{-2}s^{-1})	$Rate_{Si}$[1] (mol m^{-2}s^{-1})	Error[2] R_{Al} (%)	Error[2] R_{Si} (%)	Na (M)	I (M)	ΔG_rgibb (kcal mol^{-1})	ΔG_rqz (kcal mol^{-1})	ΔG_rkaol[3] (kcal mol^{-1})
25°C																				
KGA2-25-10	3459	0.013	3.50	3.53	1.1	5.8	0	4.8	0.97	0.9991	18.2	−2.54E-14	−2.86E-14	18	14	0	0.0004	−3.4	−0.9	−12.4
KGA2-25-10C	11187	0.013	3.57	3.46	0	5.3	0	4.3	1.13	0.9952	18.2	−2.55E-14	−2.50E-14	17	14	0	0.0004	−3.7	−1.0	−13.2
KGA2-25-11	2445	−0.012	4.02	4.07	0	5.2	0	4.1	1.07	1.0016	17.9	−2.26E-14	−2.19E-14	17	14	0	0.0001	−1.3	−1.0	−8.3
KGA2-25-11D	11186	0.012	4.00	4.03	0	3.8	0	3.3	1.11	0.9993	17.9	−1.78E-14	−1.78E-14	16	14	0	0.0001	−1.6	−1.2	−9.2
KGA2-25-1	1179	0.014	2.99	3.00	0	2.5	0	2.2	1.00	0.4005	19.1	−2.54E-14	−2.53E-14	19	17	0	0.0011	−6.1	−1.4	−18.8
KGA2-25-1C	8039	0.008	1.51	1.51	0	5.4	0	6.3	0.92	0.3992	19.1	−4.51E-14	−4.87E-14	14	15	0	0.0365	−12.4	−0.8	−30.0
KGa2-25-2	1941	0.011	3.00	2.92	0	2.4	0	2.4	0.99	0.5047	17.3	−2.58E-14	−2.59E-14	14	14	0	0.001	−6.5	−1.3	−19.4
KGA2-25-5	3255	0.009	3.00	2.96	0	3.4	0	3.4	1.02	0.4995	19.2	−2.66E-14	−2.60E-14	14	14	0	0.0011	−6.1	−1.1	−18.2
KGA2-25-6	1521	0.043	2.04	2.02	0	1.2	0	0.8	0.94	0.4021	17.9	−3.41E-14	−3.61E-14	21	16	0	0.011	−10.9	−2.0	−29.5
KGA2-25-7	465	0.044	2.50	2.47	0	0.7	0	0.6	1.16	0.4012	18.3	−3.50E-14	−3.00E-14	14	14	0	0.0034	−9.2	−2.2	−26.3
KGA2-25-7B	1636	0.012	2.50	2.46	0	1.9	0	2.0	0.94	0.4010	18.3	−2.62E-14	−2.76E-14	14	14	0	0.0034	−8.6	−1.4	−23.8
KGA2-25-8	2446	0.012	0.45	0.52	0	6.2	0	6.5	0.96	0.3011	18.4	−1.06E-13	−1.16E-13	15	14	0	0.41	−16.9	−0.8	−39.1
KGA2-25-9	2446	0.012	1.04	1.00	0	6.4	0	8.4	0.91	0.3000	18.4	−1.10E-13	−1.26E-13	15	16	0	0.1224	−14.6	−0.6	−34.2
KGA2-25-10B	6916	0.012	4.49	4.52	0	1.8	0	2.0	0.88	0.9975	18.2	−8.99E-15	−1.14E-14	16	14	0	0.0001	−0.2	−1.5	−6.9
KGA2-25-11B	3458	0.012	4.02	4.13	1.1	3.7	8	10	1.15	1.0013	17.9	−1.28E-14	−1.23E-14	20	65	0	0.0001	−1.3	−0.5	−7.3
KGA2-25-11C	6915	0.011	4.49	4.51	0	1.7	0	1.7	1.00	1.0004	17.9	−7.82E-15	−8.73E-15	16	15	0	0	−0.2	−1.5	−7.2
KGA2-25-12[i]	2618	0.008	2.93	2.95	195	206	0	7.1	1.58	1.4225	19.0	−2.65E-14	−1.76E-14	220	14	0	0.0023	−3.8	−0.7	−12.7
KGA2-25-13[i]	2618	0.012	3.00	3.01	74	83	0	7.3	1.17	1.5046	19.5	−3.00E-14	−2.53E-14	110	14	0	0.0015	−4.0	−0.7	−13.1
50°C																				
KGA2-50-1[i]	642	0.042	3.00	3.01	0	16.4	0	16	1.02	0.4042	19.2	−7.37E-13	−7.14E-13	14	14	0	0.0011	−3.3	−1.0	−11.6
KGA2-50-11A	1572	0.014	3.98	4.03	0	1.6	0	1.5	1.11	0.3998	18.3	−2.37E-14	−2.38E-14	16	14	0	0.0001	−0.4	−2.6	−8.8
KGA2-50-12C[i]	2572	0.043	3.00	2.99	0.6	18	0	16.4	1.09	0.3955	21.4	−6.63E-13	−6.79E-13	16	14	0	0.0011	−3.4	−1.0	−11.6
KGA2-50-13A[i]	1584	0.008	2.98	3.02	0	40	0	38.4	1.05	0.4973	18.7	−2.69E-13	−2.85E-13	16	14	0	0.0013	−2.7	−0.5	−9.3
KGA2-50-22[i]	500	0.037	3.02	3.02	199	207	0	1.1	6.48	0.2015	19.3	−5.79E-13	−8.83E-14	326	14	0	0.0023	−1.8	−2.7	−11.9
KGA2-50-22B[i]	1798	0.038	3.03	2.99	76	80	0	1.4	2.66	0.2009	19.3	−3.14E-13	−1.16E-13	239	14	0	0.0015	−2.4	−2.6	−12.9
KGA2-50-23[i]	842	0.042	2.98	2.99	19.7	38	0	15.6	1.21	0.5161	18.6	−6.73E-13	−5.49E-13	25	15	0	0.0013	−2.9	−1.0	−10.8
KGA2-50-23B[i]	1681	0.042	3.00	3.00	21	37	0	14	1.19	0.5121	18.6	−6.02E-13	−4.98E-13	27	15	0	0.0013	−2.9	−1.1	−10.8
KGA2-50-14	806	0.043	1.98	1.98	0	8.7	0	8.6	1.04	0.4002	18.5	−3.80E-13	−4.07E-13	16	14	0	0.0111	−8.6	−1.4	−23.0
KGA2-50-15	2621	0.009	4.00	4.04	0	3	0	2.9	0.99	0.5034	18.5	−2.06E-14	−2.32E-14	16	14	0	0.0001	0.0	−2.1	−7.2
KGA2-50-16	1420	0.047	2.48	2.47	0	7.9	0	7.6	1.04	0.4016	18.6	−4.09E-13	−3.90E-13	14	14	0	0.0034	−6.3	−1.5	−18.5
KGA2-50-17	1110	0.010	3.49	3.53	0	12.5	0	12	1.02	0.4008	18.9	−1.25E-13	−1.37E-13	16	14	0	0.0004	−1.2	−1.2	−7.7
KGA2-50-18	1104	0.023	3.49	3.52	0	7.5	0	8	0.96	0.4003	18.0	−1.99E-13	−2.05E-13	14	14	0	0.0004	−1.6	−1.5	−9.0
KGA2-50-19	2233	0.033	0.51	0.50	0	27	1	28	1.02	0.1871	19.0	−1.87E-12	−2.07E-12	16	15	0	0.4145	−15.5	−0.7	−35.1
KGA2-50-20	2233	0.036	0.99	1.00	0.9	13.3	0	12.4	1.00	0.1942	18.2	−9.50E-13	−1.06E-12	17	14	0	0.1235	−13.3	−1.2	−31.9
KGA2-50-21[i,d]	1699	0.083	3.00	3.00	0	8.3	0	7.6	1.07	0.3968	19.4	−7.10E-13	−6.78E-13	15	14	0	0.0011	−3.8	−1.5	−13.5
KGA2-50-9	699	0.047	2.02	2.01	0	8	0	8.2	0.96	0.3983	20.5	−3.29E-13	−3.82E-13	16	15	0	0.0111	−8.6	−1.5	−22.9
KGA2-50-NA-8B	2019	0.043	4.46	4.45	0	1.6	0	0.7	4.37	0.2028	19.3	−1.44E-13	−3.49E-14	14	69	0	0	1.7	−3.1	−5.6
KGA2-50-NA-1[s]	2453	0.028	1.49	1.47	0	11	0	12	0.97	0.2990	18.4	−4.81E-13	−4.92E-13	14	15	0	0.0368	−11.0	−1.2	−27.4
KGA2-50-NA-2[s]	1731	0.035	1.99	1.98	0	7.7	0	7.7	1.01	0.2982	18.5	−3.75E-13	−4.02E-13	15	14	22000	0.0336	−9.0	−1.5	−23.8
KGA2-50-NA-4[s,d]	1010	0.032	2.97	2.96	0	7.6	0	6.4	1.20	0.3001	18.2	−3.78E-13	−3.10E-13	14	14	31000	0.0322	−4.7	−1.6	−15.4
KGA2-50-NA-5[s]	2573	0.012	3.52	3.53	0	9.8	0	8.6	1.14	0.3982	18.8	−1.25E-13	−1.14E-13	15	14	31700	0.0321	−2.0	−1.4	−9.7
KGA2-50-NA-6[s]	2071	0.015	4.01	4.02	0	1.9	0	3.6	0.54	0.4032	19.4	−3.17E-14	−5.89E-14	21	14	32000	0.0321	−1.0	−2.0	−8.8
KGA2-50-NA3	1731	0.033	2.46	2.46	0	7.8	0	7	1.11	0.3007	18.7	−3.62E-13	−3.46E-13	15	14	28000	0.0317	−6.8	−1.6	−19.6
KGA2-50-NA-9[d]	2207	0.032	3.02	3.01	0	4.2	0	4	1.05	0.2048	18.5	−2.77E-13	−2.80E-13	15	14	101000	0.1113	−5.2	−1.9	−17.0
KGA2-50-NA-8[d]	2336	0.043	2.94	2.90	0	6.6	0	6.5	1.09	0.2040	19.3	−5.99E-13	−5.43E-13	14	15	1500	0.0026	−4.5	−1.6	−15.1
KGA2-50-NA-8C[d]	2479	0.039	2.96	2.94	0.9	3.5	0	3	0.90	0.2023	19.3	−1.94E-13	−2.42E-13	20	14	100000	0.1112	−6.0	−2.1	−19.2

(continued)

Table 1. Continued.

Experiment	Duration (h)	Flow rate (mL min^{-1})	pH input	pH output	Al input (μM)	Al output (μM)	Si input (μM)	Si output (μM)	$SR_{Al/Si}$	final mass (g)	BET area (m^2g^{-1})	$Rate_{Al}$ (mol m^{-2}s^{-1})	$Rate_{Si}^{(1)}$ (mol m^{-2}s^{-1})	Error$^{(2)}$ R_{Al} (%)	Error$^{(2)}$ R_{Si} (%)	Na (M)	I (M)	ΔG_rgibb (kcal mol^{-1})	ΔG_rqz (kcal mol^{-1})	ΔG_rkaol$^{(3)}$ (kcal mol^{-1})
70°C																				
KGA2-70-10	1382	0.052	1.52	1.54	0	13.8	0	14.7	0.94	0.0971	20.7	−2.96E-12	−3.14E-12	14	14	0	0.037	−9.8	−1.9	−25.1
KGA2-70-12	1775	0.081	0.53	0.52	1.4	26.6	1.1	25.2	1.04	0.0573	18.9	−1.31E-11	−1.52E-11	18	15	0	0.4189	−14.9	−1.6	−34.6
KGA2-70-13	1776	0.080	1.02	1.04	1.8	16.7	0.8	15.6	1.00	0.0706	18.9	−6.60E-12	−7.39E-12	17	15	0	0.1246	−12.3	−1.9	−30.2
KGA2-70-14A[i]	1153	0.108	3.06	3.00	0	4.2	0	4.6	0.92	0.1500	20.1	−1.14E-12	−1.38E-12	16	14	0	0.0011	−3.1	−2.7	−13.3
KGA2-70-14B[i,c]	1695	0.052	2.99	3.00	1	8.4	20	26.1	1.21	0.1489	20.1	−9.75E-13	−8.93E-13	17	62	0	0.0011	−2.6	−1.5	−10.0
KGA2-70-3[i]	984	0.043	2.98	2.99	0	11	0	11	1.01	0.1971	18.5	−9.76E-13	−1.07E-12	16	14	0	0.0011	−2.4	−2.1	−10.9
KGA2-70-6	3179	0.008	4.04	4.07	0	1.4	0	3.7	0.39	0.5015	18.0	−9.72E-15	−2.82E-14	43	14	0	0.0001	0.7	−2.9	−6.1
KGA2-70-9	1560	0.013	3.49	3.53	0	6.7	0	7.7	0.88	0.4001	18.2	−1.01E-13	−1.13E-13	14	14	0	0.0004	−0.4	−2.4	−7.2
KGA2-70-7	1560	0.033	2.49	2.51	0	58	0	55	1.06	0.3820	20.3	−2.01E-12	−1.92E-12	14	14	0	0.0037	−3.7	−1.0	−11.2
KGA2-70-5	480	0.038	2.00	2.01	0	69.5	0	65	1.07	0.3927	19.7	−2.55E-12	−2.64E-12	16	14	0	0.0115	−6.1	−0.9	−15.8
KGA270-NA-6	1810	0.038	4.48	4.47	0	1.3	0	0.5	5.44	0.0992	20.2	−1.84E-13	−3.61E-14	104	55	0	0.1013	1.5	−4.2	−7.1
KGA2-70-8A[i,c]	1091	0.022	3.01	3.05	0	16.2	51	65	1.14	0.1519	20.0	−9.90E-13	−8.68E-13	14	67	0	0.0011	−1.9	−0.9	−7.4
KGA2-70-8B[i]	1634	0.018	3.01	3.02	0	14.9	0	14.6	1.02	0.1503	20.0	−7.34E-13	−7.14E-13	14	14	0	0.0011	−2.1	−1.9	−9.8
KGA2-70-18[i]	1654	0.027	3.00	3.02	101	106	0	3.5	1.52	0.1495	18.4	−3.89E-13	−2.86E-13	258	14	0	0.0016	−0.8	−2.9	−9.2
KGA2-70-1[i]	1179	0.047	2.95	2.98	0.9	11.1	1	10.8	1.01	0.1462	18.8	−1.41E-12	−1.46E-12	15	15	0	0.0011	−2.5	−2.1	−11.0
KGA270-19[i]	1056	0.042	3.01	3.01	25	30.6	1	6.8	0.89	0.1482	19.3	−6.86E-13	−7.63E-13	63	15	0	0.0012	−1.7	−2.5	−10.0
KGA270-20[i]	965	0.044	3.01	3.04	72.6	76	0	3.1	0.99	0.1523	18.3	−4.00E-13	−4.00E-13	280	14	0	0.0015	−1.0	−3.0	−9.6
KGA270-21[i]	726	0.042	2.93	2.98	189	203	0	2.1	6.79	0.1506	17.3	−2.01E-12	−2.89E-13	157	14	0	0.0022	−0.6	−3.2	−9.5
KGA2-70-4[i]	1122	0.008	3.00	3.05	0	45	0	44	1.03	0.5022	18.4	−3.09E-13	−3.35E-13	16	14	0	0	−1.2	−1.2	−6.6
KGA2-70-15[c]	1695	0.034	3.01	3.00	0	9.8	57	68	0.92	0.1469	19.9	−8.61E-13	−1.05E-12	16	95	0	0.0011	−2.5	−0.9	−8.5
KGA2-70-16[c]	1633	0.047	3.00	2.99	0	10.4	185	197	0.93	0.1484	19.3	−1.27E-12	−1.64E-12	16	258	0	0.0011	−2.5	−0.2	−7.0
KGA2-70-17[c]	1296	0.052	3.01	2.98	0	7	564	618	0.14	0.1374	18.9	−9.71E-13	−8.99E-12	17	178	0	0.0011	−2.8	0.6	−6.2
KGA270-NA-1[s]	965	0.043	1.97	2.00	0	18.3	0	17.3	1.07	0.1021	20.9	−3.05E-12	−2.82E-12	14	15	22000	0.0337	−7.3	−1.8	−20.1
KGA270-NA-2[s]	1090	0.032	2.45	2.50	1.2	16.7	0	14.5	1.11	0.1014	20.2	−2.00E-12	−1.79E-12	15	15	28000	0.0326	−5.0	−1.9	−15.7
KGA270-NA-3[s,d]	965	0.040	2.96	2.97	1.1	8.3	0	7.4	1.03	0.0986	20.9	−1.17E-12	−1.11E-12	16	15	31000	0.0322	−3.4	−2.4	−13.3
KGA270-NA-4[s]	1063	0.017	3.48	3.58	0.8	6.8	0	6.6	0.97	0.3011	18.2	−1.58E-13	−1.62E-13	15	15	31700	0.032	−0.8	−2.5	−8.4
KGA270-NA-5[s]	2333	0.012	4.01	4.10	0	2.4	0	2.8	0.85	0.5007	18.9	−2.64E-14	−3.07E-14	14	14	32000	0.0321	0.5	−3.1	−6.8
KGA270-NA-6B[d]	2482	0.036	2.96	3.02	0	7.9	0	7.2	1.09	0.0985	20.2	−1.07E-12	−1.08E-12	16	14	100000	0.1013	−3.5	−2.4	−13.7
KGA2-70-11B	2230	0.047	2.00	2.00	0	12.2	30	46	0.77	0.1091	25.0	−1.70E-12	−2.29E-12	15	40	0	0.0112	−7.3	−1.2	−18.7

[i]: experiment designed to test the Al inhibitory effect
[s]: experiment conducted at the same Ionic strength at different pH
[d]: experiment conducted at pH 3 with different ionic strength
[c]: experiment designed to test the Si catalytic effect
(1) dissolution rate ($Rate_{Al}$ and $Rate_{Si}$) based on the release of Al and Si, respectively.
(2) error in the dissolution rate ($Rate_{A1}$ and $Rate_{Si}$), respectively.
(3)Gibbs free energy associated with the dissolution reactions of gibbsite, kaolinite and quartz, respectively.

analyzing samples with pH < 1.5, the pH was increased by adding precise amounts of 0.25 or 0.75 mol/L NaOH. The uncertainty in measured Al and Si was better than ±5% for concentrations above 4 μM. The precision dropped to ±15 and 33% for measurements at low concentrations of 2 and 0.5 μM, respectively. The pH was measured at experimental temperature on an unstirred aliquot of solution using a semi-micro 83 to 01 Orion Ross combination electrode. The reported accuracy is ±0.02 pH units (±4.5% in H^+ activities).

3. CALCULATIONS

The overall dissolution reaction of kaolinite under acidic conditions can be expressed as:

$$Al_2Si_2O_5(OH)_4 + 6H^+ \rightarrow 2Al^{3+} + 2H_4SiO_4 + H_2O \quad (3)$$

The dissolution rate, *Rate*, (mol m^{-2} s^{-1}) in steady state was based on the release of Al and Si according to the expression:

$$\nu_j \cdot Rate = -\frac{q}{A}(C_{j,out} - C_{j,inp}) \quad (4)$$

where $C_{j,inp}$ and $C_{j,out}$ are the concentrations of component j (Al or Si) in the input and the output solutions, respectively (mol m^{-3}), ν_j is the stoichiometry coefficient of j in the dissolution reaction, t is time (s), A is the surface area (m^2) and q is the fluid volume flux through the system (m^3 s^{-1}). Note that in our formalism, the rate is defined to be negative for dissolution and positive for precipitation. The error in the calculated rate (ΔR) is estimated using the Gaussian error propagation method (Barrante, 1974) from the equation:

$$\Delta P = \left[\sum_i \left(\frac{\partial P}{\partial x_i} \right)^2 (\Delta x_i^2) \right]^{1/2} \quad (5)$$

where Δx_i is the estimated uncertainty of the measurements of the quantity x_i. For most of the experiments, the error in the calculated rate ranged from 11 to 16% and is dominated by the uncertainty of the BET surface area measurement (±10%).

The degree of saturation of the solution with respect to kaolinite dissolution (Eqn. 3) is calculated in terms of the Gibbs free energy of reaction ΔG_r

$$\Delta G_r = RT \ln\left(\frac{IAP}{K_{eq}}\right) \quad (6)$$

where R is the gas constant, T is the absolute temperature, and IAP and K_{eq} are actual and equilibrium ion activity products of the solution, respectively. Using the pH, Al, Si, Na and ClO_4 total concentrations, the activity coefficients and the activities of the different species in solution were calculated using the EQ3NR code (Wolery, 1992). Errors (ΔP) in the above-calculated parameters (P), i.e., IAP and ΔG_r, were estimated according to the Gaussian error propagation Eqn. 5. Values of K_{eq} for the dissolution reactions of quartz, gibbsite and kaolinite at 25°C, 50°C and 70°C are listed in Table 2.

Table 2. Equilibrium constant (log Keq) used in ΔG_r calculations for the hydrolysis reactions of gibbsite, kaolinite and quartz.

	log Keq		
Dissolution reaction	25°C	50°C	70°C
gibbsite + $3H^+ = Al^{3+} + 3H_2O$[(1)]	7.75	6.33	5.35
kaolinite + $6H^+ = 2Al^{3+} + 2H_4SiO_4 + H_2O$[(2)]	8.95	6.4	4.61
Quartz + $2H_2O = H_4SiO_4$[(3)]	−4.63	−4.1	−3.6

[(1)]Palmer and Wesolowski (1992).
[(2)]Nagy et al. (1991).
[(3)]Robie et al. (1978).

4. RESULTS

The variations of input and output Al and Si concentrations in three representative flow-through experiments as a function of time are shown in Figure 2. Each experiment was composed of 1 to 4 stages, where each new stage was initiated by a change in the flow rate and/or the composition of the input solution. The vertical lines in the figures delineate the different stages. Much of the noise in the non-steady state data results from instabilities in flow rate. The experimental conditions of all experiments are compiled in Table 1. Al and Si concentrations are usually higher at the onset of the experiments. Afterwards, Al and Si concentrations decrease until steady state is attained (Fig. 2). Duration of experiments varies but mostly surpasses 1500 h, and some last for more than 5000 h. In general, as long as the flow rate is stable, steady state is easily maintained for several hundred hours (up to 2000 h). Several studies (e.g., Oelkers, 2000; Walther, 1996) indicate that the amount of time before steady state may influence the resulting steady-state dissolution rate. Figure 2c shows the change in Al and Si concentrations in a multi-stage experiment (KGA2-25-10) at 25°C in which the input pH varied between 3.5 and 4.5. The experiment attained the first steady state (A) after less than 2000 h. The dissolution rate at steady state was $2.7 \pm 0.3 \times 10^{-14}$ mol m^{-2} s^{-1}. After about 2000 h at steady state the pH was increased to 4.5 and a change in concentration was observed. After another 3500 h in which the pH of the input solution was 4.5 most of the time, input pH was changed back to 3.5. New steady state at pH 3.5 was achieved after another 3000 h. The dissolution rate at this last steady state was $2.5 \pm 0.3 \times 10^{-14}$ mol m^{-2} s^{-1}, which is (within error) the same dissolution rate as that of stage A. We did not observe a systematic gradual decrease with time neither of Al nor of Si output concentrations, as reported by Brantley et al. (1995) for feldspar dissolution with flow-through experiments.

Kaolinite dissolution rates (Eqn. 4) were obtained based on the release of silicon ($Rate_{Si}$), and aluminum ($Rate_{Al}$) at steady state, for each flow-through experiment (Table 1). Figure 3 plots the dissolution rates evaluated based on the release of Si versus those obtained based on the release of Al. The solid lines in Figure 3 are the 1/1 diagonal. Taking into account the appropriate errors, Figure 3 shows good agreement between the different estimates of kaolinite dissolution rate. The stoichiometric ratio between Al and Si ($SR_{Al/Si}$) is defined as the ratio between the release of Al and the release of Si at steady state:

$$SR_{Al/Si} = \frac{C_{Al,out} - C_{Al,inp}}{C_{Si,out} - C_{Si,inp}} \quad (7)$$

where $C_{i,inp}$ and $C_{i,out}$ are the concentrations of component i in the input and the output solution, respectively. For most experiments the Al/Si stoichiometric ratio ranges between 0.9 and

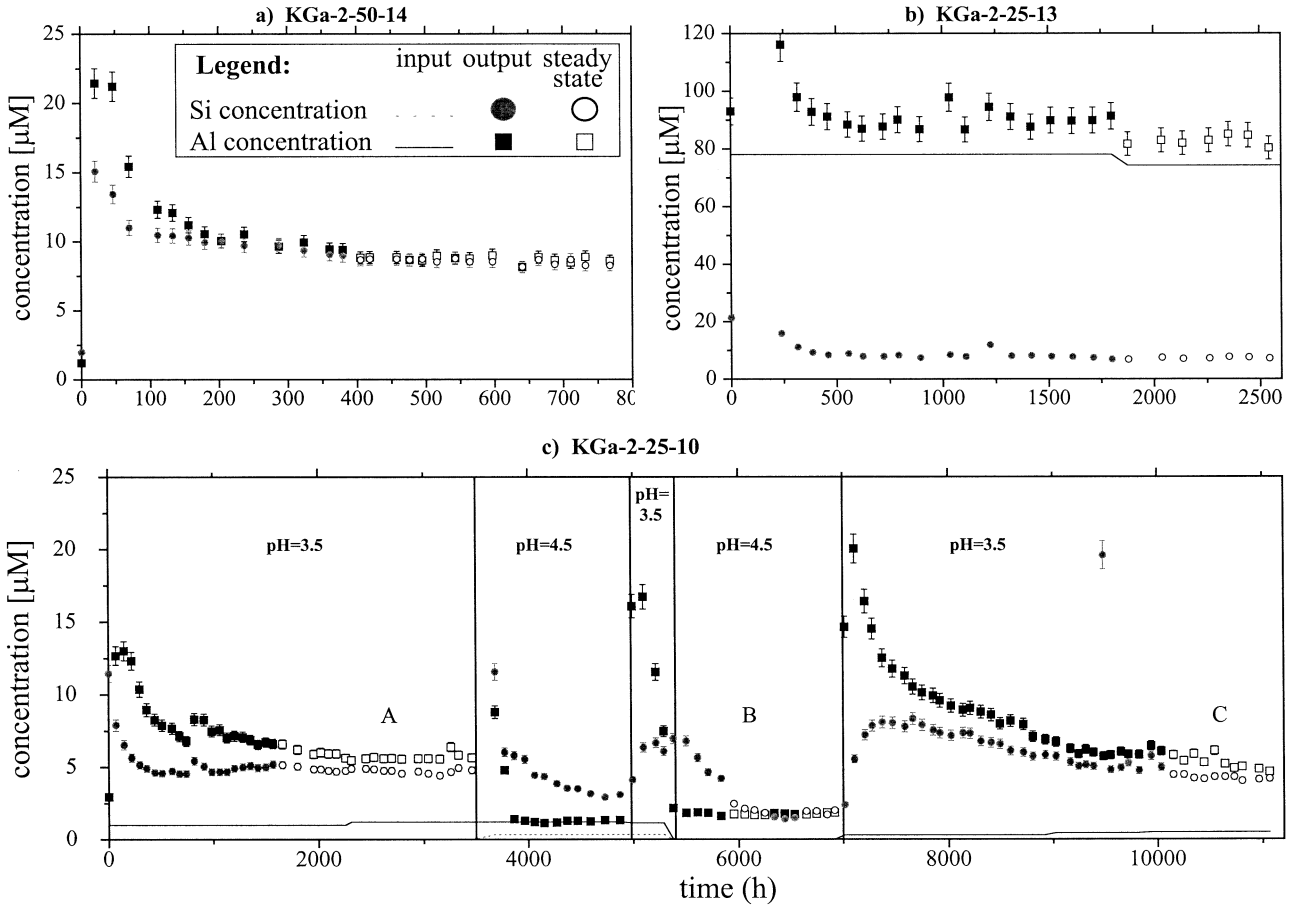

Fig. 2. Variation in Al and Si concentration as a function of time in three representative experiments. The vertical lines represent changes in experimental conditions between the different stages. Al and Si values used to calculate average steady state are denoted by open symbols.

1.2 (Table 1). The exceptions are experiments in which the silicon or aluminum output concentrations were either very low ($<4\mu$M) or similar to the input concentration. In both cases, the error on the calculated rates (Table 1) and on the stoichiometric ratio is very high. To minimize errors, dissolution rate is calculated as the average of $Rate_{Al}$ and $Rate_{Si}$ in all experiments in which the error associated with both is less than 20% (Table 1). In the rest of the experiments, we used either $Rate_{Al}$ or $Rate_{Si}$, whichever had the smaller error.

All the steady-state dissolution rates are measured at conditions of undersaturation with respect to quartz and gibbsite. Exceptions are experiments conducted at pH of about 4 and 4.5 at 50°C and 70 °C in which equilibrium with respect to gibbsite is achieved (Table 1) and, consequently, incongruent dissolution occurs due to Al depletion. In these experiments the dissolution rate is based only on Si release (see Table 1). In the experiments conducted to determine a possible Si inhibitory/catalytic effect at 70 °C and pH 3, the Si output concentration ranges from 10 to 620 μM (Table 1). Few of the experiments with very high Si concentration showed supersaturation with respect to quartz. For those experiments dissolution rates were based only on Al release.

In the present study the observed steady-state kaolinite dissolution rates range, as a function of temperature and fluid composition, from 8×10^{-15} mol m^{-2} s^{-1} (at 25°C and pH 4.5) to 1.5×10^{-11} mol m^{-2} s^{-1} (at 70°C and pH 0.5).

5. DISCUSSION

5.1. Separating the Direct Effects of pH and Temperature from Effects of Other Environmental Variables

Figure 4 shows log dissolution rate versus pH at 25°C, 50°C and 70°C. Although the observations may be described by Eqn. 1 reasonably well, as is evident by the linear trends in Figure 4, detailed examination of the data shows that three trends may be characterized in log rate vs. pH plots. At 25°C (Fig. 4a) the rate increases when the pH decreases from 4.5 to 3.5, remains relatively constant between pH 3.5 and 2.5 and increases again towards pH 1. Similar trends are observed at 50°C and 70°C (Fig. 4b and c), although the transition between the linear range to the range in which the rate is pH independent is shifted towards more acidic pH as the temperature increases.

To model the effect of pH and temperature on kaolinite dissolution rate it is important to separate between direct and indirect effects of the environmental variables involved. By direct effect we mean an effect related to surface processes and

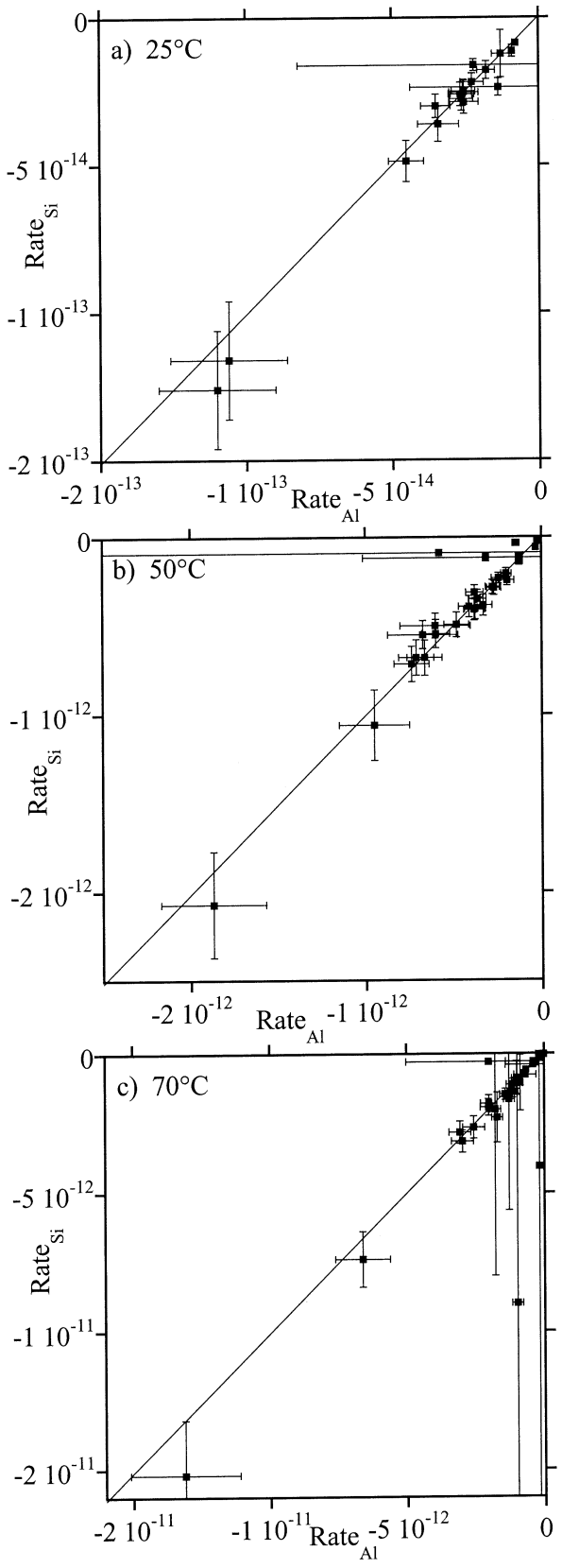

Fig. 3. Comparison dissolution rates evaluated based on the release of Al, $Rate_{Al}$, with those obtained based on the release of Si, $Rate_{Si}$. The solid lines are the 1/1 diagonal.

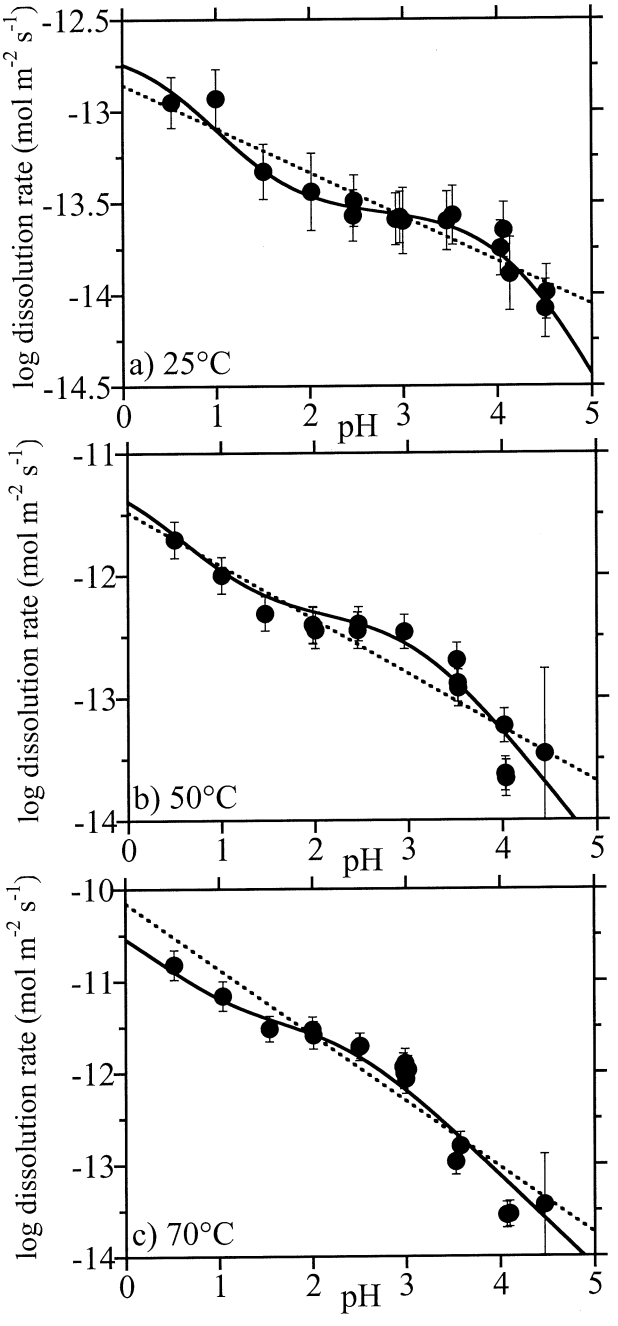

Fig. 4. Variation of log dissolution rate with pH: (a) at 25°C, (b) at 50°C and (c) at 70°C. The dashed curves and the solid curves are a result of linear regression and multiple non-linear regression of Eqn. 17, respectively, to the measured rate data at 25°C, 50°C and 70°C.

therefore, one that can be used to understand the reaction mechanism. For example, the direct effect of pH on dissolution rate is typically attributed to the effect of the adsorbed proton on bond strength. In this example, "separation of variables" implies that this effect of the adsorbed proton is independent of temperature. An example of an indirect effect is the effect of pH on rate as a result of changes in the degree of saturation. This indirect effect depends, among other things, on the temperature (Cama et al., 1999). In addition to temperature and pH,

other environmental variables such as output Al concentration, ionic strength and the degree of saturation, vary between the experiments. Therefore, their possible effects on the kaolinite dissolution rate are examined below.

5.1.1. Aluminum inhibition

Oelkers et al. (1994) and Devidal et al. (1997) show a strong aluminum inhibition of kaolinite dissolution rate at 150°C at saturated vapor pressure and pH = 2. The Al inhibits the dissolution reaction even under very far from equilibrium conditions. As the Al output concentration in experiments conducted under different temperatures and pH varied, the Al effect should be taken into account in the interpretation of the effects of pH and temperature. Figure 5a shows the effect of aluminum on kaolinite dissolution rate obtained in the present study mostly at pH = 3 and temperatures of 25°C, 50°C and 70°C and from Oelkers et al. (1994) at pH = 2 and 150°C. Whereas a significant inhibitory effect is observed at 50°C and 70°C (at pH = 3), aluminum hardly affects dissolution rate at 25°C. Different mechanistic models were proposed in the literature for the inhibition of kaolinite dissolution rate at 150°C by aluminum (Devidal et al., 1997; Ganor and Lasaga, 1998). All of these models may be adequately applied to the aluminum inhibition observed at 50°C and 70°C. The currently available data on aluminum inhibition are not sufficient to prefer one mechanistic model over the others.

To compare the effect of aluminum on dissolution rate at different temperatures we normalized the dissolution rates by dividing the dissolution rates at each temperature and pH by the dissolution rate obtained at the same temperature and pH with minimum aluminum concentrations (2.4, 16, 4.2 and 4.3 μM Al^{3+} at 25°C, 50°C, 70°C and 150°C, respectively). Figure 5b shows log normalized dissolution rate versus log Al^{3+}. At pH = 3 the effect at 50°C and 70°C is significantly stronger than that at 25°C. The aluminum inhibition at 150°C and pH = 2 (after Oelkers et al., 1994) seems to be stronger than those at 50°C and 70°C at pH = 3, although there is a significant scatter in the high aluminum concentration data at 150°C. The effect of aluminum on kaolinite dissolution rate at pH other than 3 was not thoroughly examined in the present study. Based on two data points at pH = 2 and two data points at pH 2.5, it seems that at 70°C the inhibition effect is less significant at these pHs than at pH = 3 (Fig. 5a). Certainly, more experimental data are needed to explain the effect of aluminum on kaolinite dissolution rate and to include it in a full rate law. This is beyond the scope of the present paper, however.

The range of aluminum concentrations in the experiments that were used to examine the effect of pH on dissolution rate at 25°C (Fig. 4a) is $1\cdot10^{-6}$ to $6\cdot10^{-6}$ M. As can be seen in Fig. 5 dissolution rate at 25°C and pH 3 is not affected by changes in aluminum concentration of up to $8\cdot10^{-5}$ M. The range of aluminum concentrations in the experiments that were used to examine the effect of pH on dissolution rate at 50°C and 70°C (Fig. 4b and c) is $1\cdot10^{-6}$ to $1\cdot10^{-5}$ M, for experiments conducted at pH = 3 to 4.5. If the aluminum inhibition at pH 3 to 4.5 is similar to that observed at pH 3 (Fig. 5), then the rates shown on Figures 4b and c at this pH range are inhibited by up to 10% at 50°C and by up to 25% at 70°C. At pH 0.5 to 2.5 at 50°C and 70°C (Fig. 4b and c) the range of aluminum concentrations in the experiments is $7\cdot10^{-6}$ to $2.7\cdot10^{-5}$ M. If the aluminum inhibition at pH 0.5 to 2.5 is similar to that observed at pH 3 (Fig. 5), then the rates shown on Figures 4b and c at this pH range are inhibited by up to a factor of 2 at 50°C and up to a factor of 3 at 70°C. However, four experiments conducted at pH = 2 and 2.5 (Fig. 5a), show no significant aluminum effect on kaolinite dissolution rate at 70°C. Therefore, it seems that using the pH 3 data to estimate the possible effect of aluminum on dissolution rate below pH 3 would overestimate the effect.

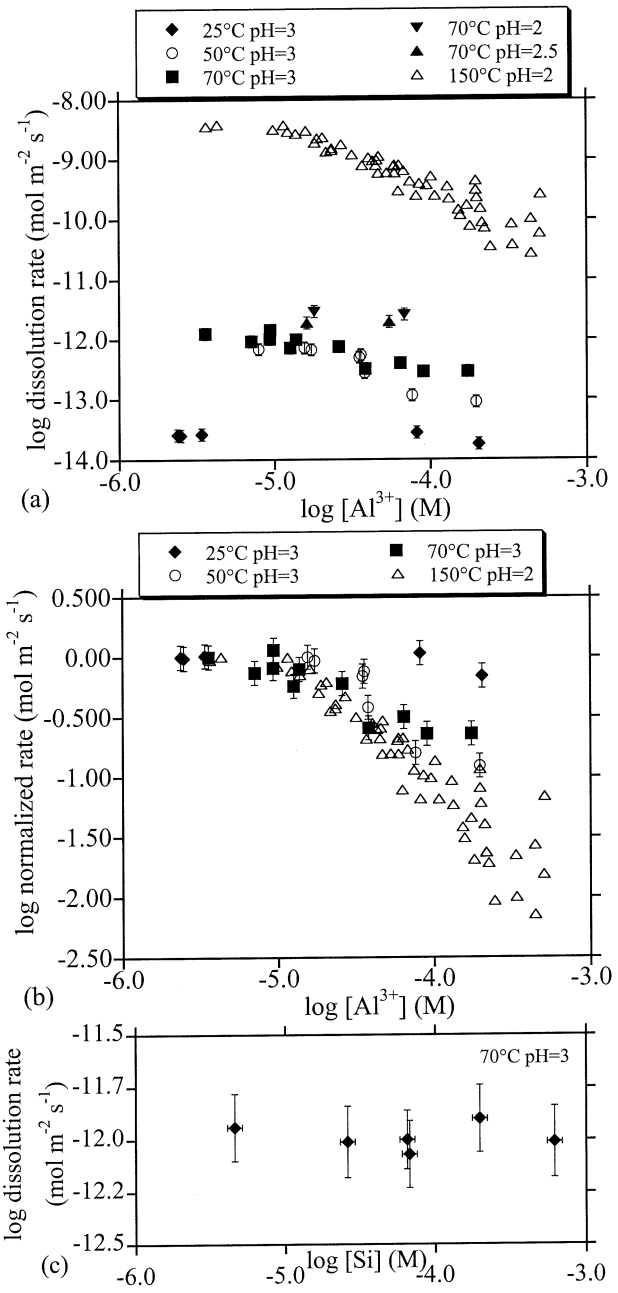

Fig. 5. The effect of aluminum (a and b) and silicon (c) on kaolinite dissolution rate. The data at 150°C is from Oelkers et al. (1994). The dissolution rates in (b) are normalized by dividing the measured dissolution rates by the dissolution rate obtained at the same temperature and pH with minimum aluminum concentrations.

Due to the relatively low aluminum concentrations in the experiments that were used to examine the effect of pH on dissolution rate in the present study, the aluminum effect on the general shape of the log rate vs. pH plot (Fig. 4) is relatively small. Therefore, in the following discussion we use the measured rates in our model, without attempting to correct for the effect of aluminum inhibition.

5.1.2. The effect of silicon

Figure 5c shows that increasing Si concentration in solution from less than 5 μM to more than 600 μM at pH 3 and 70°C does not affect the dissolution rate. This is in agreement with the results of Devidal et al. (1997), in which the presence of Si in acidic conditions neither inhibits nor catalyzes the kaolinite dissolution reaction.

5.1.3. The effect of degree of saturation

The ΔG_r of the kaolinite dissolution reaction is a strong function of pH and of Al and Si concentrations. If the dissolution rate varied due to changes in ΔG_r in the different experiments, as the pH and the output concentrations varied, then the calculated pH reaction order will include a spurious contribution. This problem would be minimal only in the "far-from-equilibrium" dissolution plateau region, which is defined as the region in rate vs. ΔG space where there is no direct effect of the degree of saturation on dissolution rate. As the dissolution rate of kaolinite is directly affected by the pH and the aluminum concentration, changes in pH and aluminum will cause an indirect effect of the degree of saturation on dissolution rate. In contrast to aluminum, silicon does not affect dissolution rate under far from equilibrium conditions. Therefore, the direct effect of the degree of saturation on dissolution rate, may be examined by manipulating the silicon concentration, as was done by Nagy et al. (1991). Nagy et al. (1991) have shown that the dissolution plateau for *kaolinite* at 80°C is reached for $\Delta G_r < -2$ kcal/mol, i.e., for ΔG_r below -2 kcal/mol kaolinite dissolution rate is not directly affected by the degree of under saturation. The results of Mogollon et al. (1996) show that the dissolution plateau for gibbsite at 25°C is in very good agreement with the results of Nagy and Lasaga (1992) at 80°C. Assuming that the dissolution plateau for kaolinite is similarly independent of temperature, our experimental range of ΔG_r, namely -5.6 to -39 kcal/mol (Table 1), is well within the dissolution plateau. Therefore, our dissolution rates should be independent of the deviation from equilibrium.

5.1.4. The effects of ionic strength, Na^+ and ClO_4^-

One of the advantages of flow-through experiments is that the pH is maintained constant at steady state by the balance between the H^+ consumption and the differences in pH between the input and output solution. Therefore, it enables the determination of the dissolution rate at a constant pH, without requiring a pH-stat or buffers that may influence the reaction rate. All the experiments at 25°C and some of the experiments at 50°C and 70°C were performed under relatively low ionic strength conditions using different concentrations of $HClO_4$ solutions. The drawback of such an experimental setting is that changing the acid concentration changes both the pH and ClO_4^- concentration. The solution ionic strength in these experiments ranges from 0.000032 mol/L (pH 4.5) to 0.32 mol/L (pH 0.5). Thus the lower the pH, the higher the ionic strength. As a consequence, enhancement of dissolution rates as pH decreases may be affected by an increase in the ionic strength or in ClO_4^- concentration. To study these effects a second set of experiments was conducted at 50°C and 70°C and pH range of 1.5 to 4. In this set a constant ionic strength and ClO_4^- concentration of ~0.032 mol/L was maintained by adding suitable amounts of $NaClO_4$ into the input solutions (Table 1). By doing this, Na^+ concentration increases as the pH increases whilst ClO_4^- concentration remains constant (~0.032 mol/L). Figure 6 compares dissolution rates in experiments conducted under constant ionic strength to those obtained without adding $NaClO_4$, i.e., where $H^+ = ClO_4^-$. In all experiments at 70°C and most experiments at 50°C the two sets show the same dissolution rates. The exceptions are the 50°C experiments at pH = 3 and 4. At pH = 3 the dissolution rate is slower in the experiment in which $NaClO_4$ was added, than in those experiments where the input solution contain only $HClO_4$. At pH = 4 an opposite trend is observed, i.e., the dissolution rate is slower in the experiment that contains $NaClO_4$. Currently, we do not have a sound explanation for these effects. For the purpose of modeling the effects of pH and temperature we decided to use primarily the rates that were obtained under constant ionic strength, but include in the data set some experiments that were conducted under conditions in which $H^+ = ClO_4^-$. As the effect on the rate is small to insignificant, the results of the modeling will be only slightly influenced by this decision.

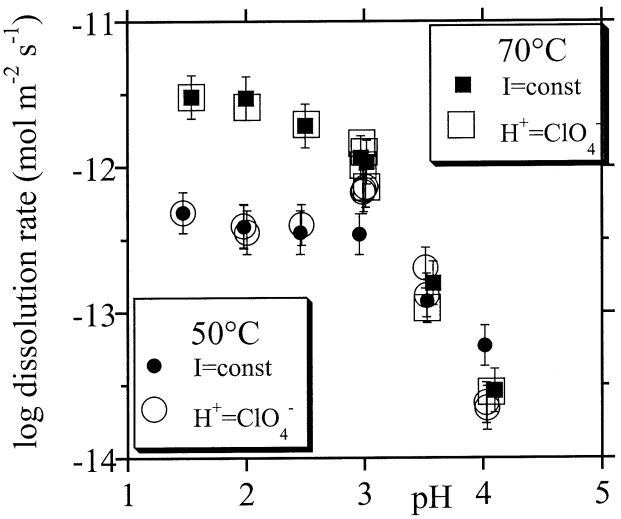

Fig. 6. Comparison of dissolution rates in experiments conducted under constant ionic strength and ClO_4^- concentration of ~ 0.032 mol/L with those obtained without adding $NaClO_4$, i.e., where $H^+ = ClO_4^-$ (see text).

5.2. The Effect of pH on Dissolution Rate

To describe a full rate law of a reaction, it is important to determine how many mechanisms control the reaction rate under the examined range of environmental conditions. As the

observed pH dependence of the rate may be described by a linear trend on a log rate vs. pH plot (Fig. 1), the reaction may be modeled reasonably well using Eqn. 1 and a single proton-promoted reaction mechanism. Any attempt to use a more complicated model, in which the rate is governed by two (or more) reaction mechanisms, is justified only if one shows that the changes in slope with pH, on the log rate vs. pH plot, are significant and do not reflect experimental noise. Close examination of the data (Fig. 4) clearly shows that the slope varies with pH at all temperatures and that the rate is constant or almost constant in an intermediate pH range. To support this observation we conducted duplicates and triplicates of some of the experiments in this intermediate stage, and as can be seen in Figure 4, the scatter of the replicates is relatively small, indicating that the observed plateau is significant. Moreover, similar ranges in which kaolinite dissolution rate under acidic conditions is independent of pH were obtained in previous studies (e.g., Wieland and Stumm, 1992; Ganor et al., 1995). Therefore, we suggest that the overall dissolution rate of kaolinite under acidic conditions is governed by two reaction mechanisms.

5.2.1. *The proposed model*

The following model is based on three assumptions: 1) Kaolinite dissolution rate under acidic conditions is controlled by two independent parallel reaction paths; 2) Each reaction path consists of fast adsorption of a proton on a different surface site followed by a slow hydrolysis step; 3) The adsorption of the protons on each of these surface sites may be described by a simple independent Langmuir adsorption isotherm:

$$X_{i,ads} = F_i \frac{b_i \cdot a_{H^+}}{1 + b_i \cdot a_{H^+}} \tag{8}$$

where F_i is the maximum surface coverage of protons on site i, b_i is a constant related to the energy of adsorption on site i and a_{H^+} is the activity of protons in solution.

Adsorption of a proton on a surface site close to the metal influences the bond strength and thus affects the dissolution rate. If steady-state conditions are maintained, the rate of this reaction path is (Lasaga, 1981):

$$\frac{Rate_i}{\rho r} = k_i \cdot X_{i,ads} \tag{9}$$

where k_i (s^{-1}) is the rate coefficient of this path, ρ_r (mol m^{-2}) is the density of reactive surface sites on the mineral surface and $X_{i,ads}$ is the molar fraction of the surface site that is protonated. Substituting the Langmuir adsorption isotherm (Eqn. 8) into Eqn. 9, gives:

$$\frac{Rate_i}{\rho r} = k_i \cdot F_i \frac{b_i \cdot a_{H^+}}{1 + b_i \cdot a_{H^+}} \tag{10}$$

As the two parallel reaction paths are independent of each other, the overall dissolution rate will be the sum of the rates of the two paths, i.e.,

$$\frac{Rate}{\rho r} = k_1 \cdot F_1 \frac{b_1 \cdot a_{H^+}}{1 + b_1 \cdot a_{H^+}} + k_2 \cdot F_2 \frac{b_2 \cdot a_{H^+}}{1 + b_2 + a_{H^+}} \tag{11}$$

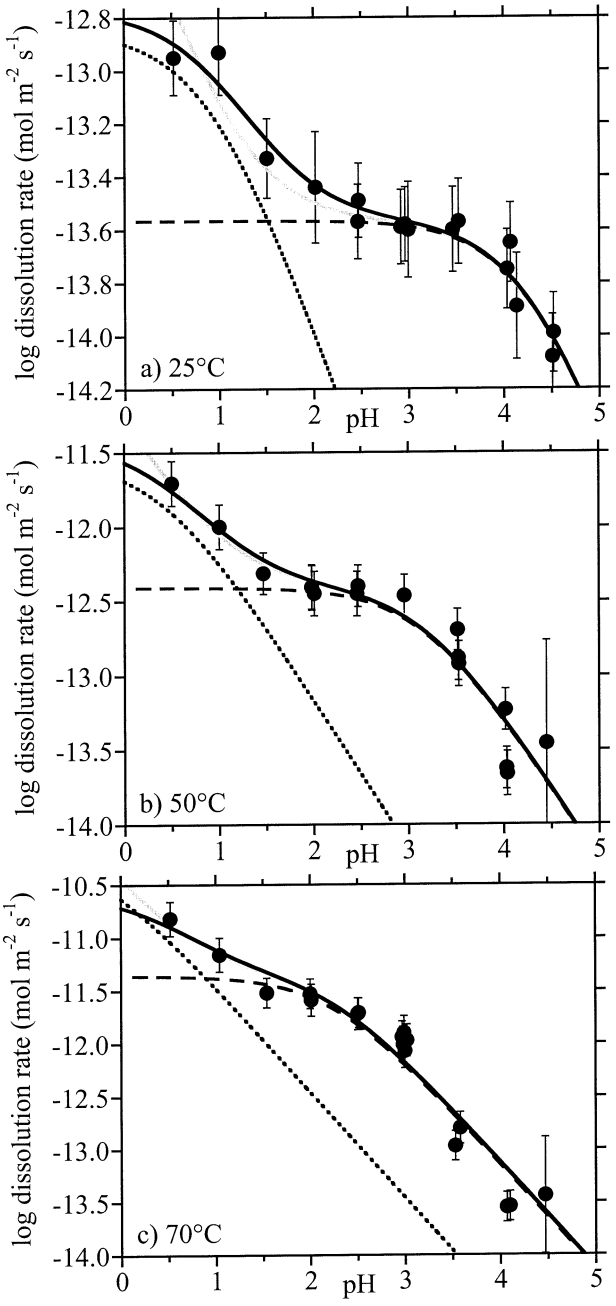

Fig. 7. Comparison of the prediction (black solid curves) of the proposed model at constant temperature (Eqn. 11) with the measured dissolution rates at (a) 25°C, (b) 50°C, and (c) 70°C. The dotted line and the dashed line are plots of the first and the second terms in Eqn. 11, respectively, i.e., of the pH dependencies of the two reaction paths (see text). The solid gray curves are curve fits that were achieved with very small b_2 (see text).

5.2.2. *Fitting the proposed model to the experimental data*

For each temperature, the coefficients $k'_1 = k_1 F_1 \rho_r$, $k'_2 = k_2 F_2 \rho_r$, b_1 and b_2 were calculated from a non-linear regression of Eqn. 11 using least squares (Fig. 7). For the 25°C the black solid line in Fig. 7a is the best-fit curve that is described by:

$$Rate_{25°C} = 2.7 \cdot 10^{-14} \cdot \frac{18000 \cdot a_{H^+}}{1 + 18000 \cdot a_{H^+}} + 1.4 \cdot 10^{-13} \cdot \frac{7.7 \cdot a_{H^+}}{1 + 7.7 \cdot a_{H^+}} \quad R^2 = 0.96 \quad (12)$$

The dotted line and the dashed line are plots of the first and the second terms in Eqn. 12, respectively, i.e., of the pH dependencies of the two reaction paths. As can be seen, the first reaction path solely dominates the overall rate above pH 2.5. Between pH 2.5, in which 89% of the rate is due to the first reaction path, and pH 1, in which only 30% of the rate is due to the first reaction path, the two reaction paths influence the rate. Only at pH 0.5, the second reaction path solely dominates the overall rate. As a result, the fitting of the experimental data to the first reaction path is much more sound than the fitting to the second reaction path. Therefore, different combinations of the two coefficients in the second term yield similar curves that adequately describe the experimental data. For example, the gray solid line in Figure 7a was obtained by replacing k'_2 and b_2 with values of 10^{-8} and $5 \cdot 10^{-5}$, respectively.

The small value of b_2 ($5 \cdot 10^{-5}$) implies that at pH 1 less than 0.002% of the available sites are protonated. It is not very probable that the overall rate will be dominated by the second reaction path when such a small fraction of the site is protonated. Therefore, although both curves adequately describe the experimental data, Eqn. 12 is much more reasonable. At 50°C and 70°C the best-fit curves (solid gray curves in Figs. 7b and c) were achieved with a very small b_2 value. Therefore, in fitting the experimental data we force the value of b_2 to be 2, so 40% of the second reaction site would be protonated at pH 1. The resulting curves (solid black curves in Figs. 7b and c) are almost identical to the best fit curves (gray curves) and are described with the following coefficients: at 50°C ($R^2 = 0.92$) $- k'_1 = 3.9 \cdot 10^{-13}$, $k'_2 = 3.5 \cdot 10^{-12}$, $b_1 = 1500$ and $b_2 = 2$; at 70°C ($R^2 = 0.94$) $- k'_1 = 4.2 \cdot 10^{-12}$, $k'_2 = 2.3 \cdot 10^{-11}$, $b_1 = 170$ and $b_2 = 2$.

5.3. The Effect of Temperature on Dissolution Rate

The temperature dependence of the dissolution rate generally follows the Arrhenius law:

$$Rate = Ae^{-E_a/RT} \quad (13)$$

where A is the preexponential factor, E_a is the apparent activation energy, R is the gas constant and T is the temperature (K). To obtain the apparent activation energy experimentally, it is common to conduct several experiments at different temperatures while all the other experimental variables (e.g., pH) are held constant. By plotting the natural log of these dissolution rates vs. 1/T, an apparent activation energy may be calculated using Eqn. 13 from a least squares estimate of the slope of the plot (Fig. 8a). A critical assumption in calculating activation energies using this method is that the preexponential factor, A, is the same in all experiments. This preexponential factor includes other effects of the experimental variables on the rate. As mineral dissolution is a surface process, the pH effect on dissolution rate is controlled by protons adsorbed on the surface (Eqn. 2) and not directly by the pH. Therefore, conducting experiments under the same pH is not enough to keep the preexponential factor constant, and one should keep the surface concentration constant. Figure 8b plots the change in molar fraction of the proton surface coverage of the first surface site as a function of pH at 25°C, 50°C and 70°C as predicted by the proposed model, i.e., by the best fit of the Langmuir part of the first term in Eqn. 11. As the pH dependence of the surface coverage varies with temperature, dissolution rates at the same

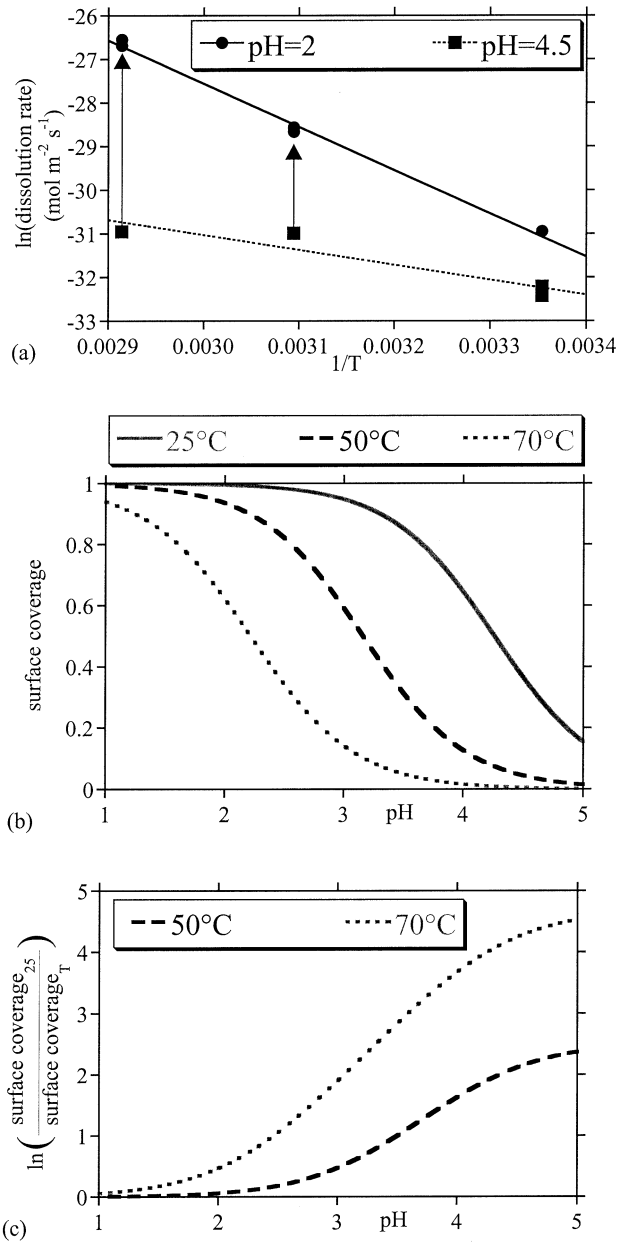

Fig. 8. (a) Arrhenius plots of kaolinite dissolution calculated at constant pH of 2 and 4.5. The arrows show the correction needed to change the Arrhenius plot at constant pH of 4.5 to an Arrhenius plots at constant surface coverage of protons. (b) The change in molar fraction of the proton surface coverage of the first surface site as a function of pH as is predicted by the proposed model (c) The natural log of the ratio between the surface coverage at 50°C and 70°C and the surface coverage at 25°C, which may be used as correction for Arrhenius plot calculated for constant pH.

pH and different temperatures are influenced by different proton concentrations on the surface. For example, at pH 4.5 the proton surface coverage is 36%, 4% and 0.5% at 25°C, 50°C and 70°C, respectively. If the dissolution rate is linearly proportional to the surface coverage it is possible to predict the dissolution rate at a certain surface coverage (y) based on rate measured at another surface coverage (x) from the equation:

$$Rate_{(H^+_{ads=y})} = Rate_{(H^+_{ads=x})} \cdot \frac{y}{x} \tag{14}$$

For example, to calculate the dissolution rate at 50°C and 70°C under the same surface coverage as at 25°C (i.e., 36%) the rate should be multiplied by factors of 9 (=36/4) and 72 (=36/0.5), respectively. The natural log of the correction to the surface coverage at 25°C, i.e., the ln of the ratio between the surface coverage at 50°C and 70°C and the surface coverage at 25°C, is plotted as a function of pH in Fig. 8c. The proton surface coverage at 25°C and pH = 2 is similar to those at 50°C and 70°C at the same pH (Fig. 8b) and therefore the corrections are small (Fig. 8c), and the slope of the Arrhenius plot (Fig. 8a) is acceptable. At pH 4.5 on the other hand, Figure 8c shows that the natural log of the dissolution rate on the Arrhenius plot at 50°C and 70°C should be shifted upwards by 2.1 and 4.1 U, respectively, to obtain activation energy under constant surface coverage. Such a shift (arrows on Fig. 8a) will result in a major change in the slope of the Arrhenius plot and the calculated activation energy. We suggest that the pH dependence of the apparent activation energy that was observed by Carroll and Walther (1990) is an artifact of the differences in the pH dependence of the proton surface coverage at different temperatures.

A pH-independent apparent activation energy for each of the reaction paths is calculated by plotting an Arrhenius plot (Fig. 9a) of the rate coefficients (k'_1 and k'_2) at 25°C, 50°C and 70°C, which were obtained from the fitting of the experimental data to the proposed model (Eqn. 11). The obtained activation energies are 23 ± 1 and 23 ± 2 kcal/mol for the first and the second reaction path, respectively. For both reaction paths, the Arrhenius plots show excellent linearity ($R^2 > 0.99$). It is important to note that the excellent linearity of the Arrhenius plot was achieved, even though the rate coefficients of the first reaction path were determined independently at 25°C, 50°C and 70°C, based on the experimental data and the proposed model. This good linearity and the reasonable value of the activation energy provide independent support for the proposed model. As was discussed earlier, the rate coefficients of the second reaction path are not well constrained by the data, and therefore the activation energy calculated from these coefficients is even less constrained.

5.4. The Combined Effect of pH and Temperature on kaolinite Dissolution Rate

The apparent activation energies discussed above were determined from a best-fit of rate coefficients that were obtained by fitting the experimental results at each temperature. Alternatively, it is possible to fit the entire data set to a combined equation that describes both effects of pH and temperature.

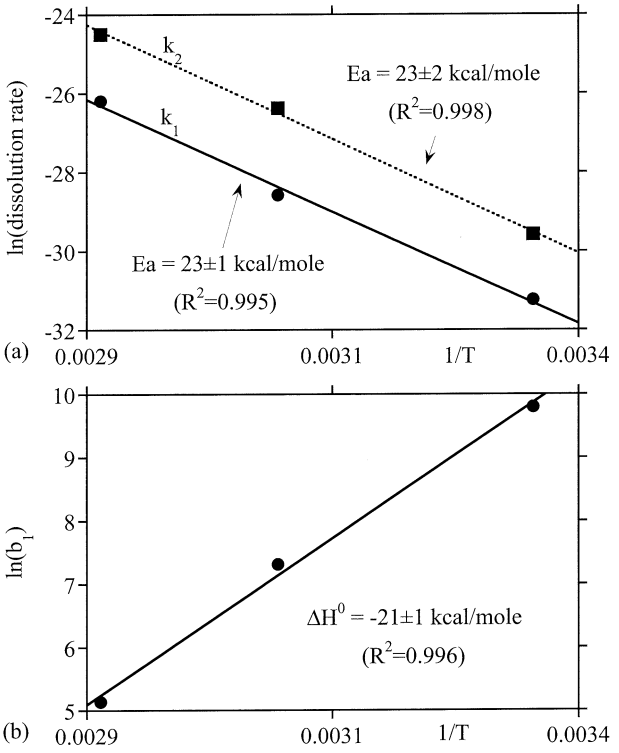

Fig. 9. (a) Arrhenius plots of kaolinite dissolution calculated from the rate coefficients that were obtained from the fitting of the experimental data to the proposed model (Eqn. 11). (b) Plot of natural log of the *b* coefficients of the first reaction path that were obtained from the fitting of the experimental data to the proposed model (Eqn. 11) versus the temperature reciprocal.

Substituting the rate coefficients in Eqn. 11 by Arrhenius terms (Eqn. 13) gives,

$$\frac{Rate}{\rho r} = A_1 \cdot e^{-E_{a_1}/RT} \cdot F_1 \frac{b_1 \cdot a_{H^+}}{1 + b_1 \cdot a_{H^+}} + A_2 \cdot e^{-E_{a_2}/RT} \cdot F_2 \frac{b_2 \cdot a_{H^+}}{1 + b_2 \cdot a_{H^+}} \tag{15}$$

As b_1 and b_2 are constants related to the energy of proton adsorption on their respective sites, their values depend on temperature. This temperature dependence may be evaluated recalling that the *b* constant in the Langmuir adsorption isotherm is the equilibrium constant of the protonation reaction and therefore its temperature dependence may be written as:

$$b = e^{\Delta S^0/R} \cdot e^{-\Delta H^0/RT} = K_0 \cdot e^{-\Delta H^0/RT} \tag{16}$$

where ΔS^0 (cal mol^{-1} K^{-1}) is the entropy, and ΔH^0 (kcal mol^{-1}) is the net enthalpy of adsorption. Following Sverjensky and Sahai (1998), the standard states for both surface and aqueous species are assumed to reflect hypothetical 1 molal solutions referenced to infinite dilution and a surface potential of zero at 25°C. The temperature dependence of the *b* constant in the Langmuir adsorption isotherm may be described using Eqn. 16 and assuming that the heat capacity, ΔC_p, is equal to zero, and therefore ΔH^0 is temperature independent. This last assumption may be examined by plotting the natural log of the

b coefficients of the first reaction path at 25°C, 50°C and 70°C, which were obtained from the fitting of the experimental data to the proposed model (Eqn. 11), versus the temperature reciprocal (Fig. 9b). The linearity of the plot indicates that the temperature dependence of the calculated *b* coefficients is properly described by Eqn. 16 with constant ΔH^0. The net enthalpy of adsorption on the first surface site is calculated by multiplying the slope of the regression line in Fig. 9b by the gas constant, and found to be $\Delta H^0 = -21 \pm 1$ kcal/mol. This value is within the range of -7.9 to -23.1 kcal/mol, experimentally obtained for oxides (Sverjensky and Sahai, 1998). The reasonable temperature dependence of the *b* coefficients is yet another indication for the validity of the proposed model. Since the fitting coefficients of the second reaction path are poorly constrained, they are not adequate for calculation of adsorption enthalpy.

The estimation of ΔH^0 discussed above was done in two stages: first, the *b* values were obtained by fitting the experimental data at each temperature to Eqn. 11; and second, ΔH^0 was obtained by fitting the *b* values to Eqn. 16. To fit the whole data set into a single equation, Eqn. 16 is substituted into Eqn. 15:

$$\frac{Rate}{\rho r} = A_1 \cdot e^{-E_{a_1}/RT} \cdot F_1 \frac{K_{0_1} \cdot e^{-\Delta H_1^0/RT} \cdot a_{H^+}}{1 + K_{0_1} \cdot e^{-\Delta H_1^0/RT} \cdot a_{H^+}} + A_2 \cdot e^{-E_{a_2}/RT} \cdot F_2 \frac{K_{0_2} \cdot e^{-\Delta H_2^0/RT} \cdot a_{H^+}}{1 + K_{0_2} \cdot e^{-\Delta H_2^0/RT} \cdot a_{H^+}} \quad (17)$$

Eqn. 17 describes the combined effect of pH and temperature on kaolinite dissolution rate. The coefficients $k''_1 = A_1 F_1 \rho_r$, $k''_2 = A_2 F_2 \rho_r$, E_{a1}, E_{a2}, K_{01}, K_{02}, ΔH_1^0 and ΔH_2^0 were calculated from a multiple non-linear regression of Eqn. 17 using least squares. The resulting coefficients are $k''_1 = 200$ mol m^{-2} s^{-1}, $k''_2 = 5 \cdot 10^7$ mol m^{-2} s^{-1}, $E_{a1} = 22$ kcal mol^{-1}, $E_{a2} = 28$ kcal mol^{-1}, $K_{01} = 2 \cdot 10^{-10}$, $K_{02} = 1.4 \cdot 10^{-7}$, $\Delta H_1^0 = -19$ kcal mol^{-1} and $\Delta H_2^0 = -10$ kcal mol^{-1}. The regression coefficient is $R^2 = 0.97$. Substituting these values into Eqn. 15 yields,

$$Rate = 2 \cdot 10^2 \cdot e^{-22/RT} \cdot \frac{2 \cdot 10^{-10} \cdot e^{19/RT} \cdot a_{H^+}}{1 + 2 \cdot 10^{-10} \cdot e^{19/RT} \cdot a_{H^+}} + 5 \cdot 10^7 \cdot e^{-28/RT} \cdot \frac{1.4 \cdot 10^{-7} \cdot e^{10/RT} \cdot a_{H^+}}{1 + 1.4 \cdot 10^{-7} \cdot e^{10/RT} \cdot a_{H^+}} \quad (18)$$

A comparison between the prediction of Eqn. 18 and the experimental data at 25°C, 50°C and 70°C is shown in Fig. 4.

A by-product of the model fitting (Eqn. 18) is that it predicts the molar fraction of protonated sites on each of the two surface sites. Ganor et al. (2002) compared this prediction to protonation data obtained from surface titration, and found an excellent agreement between the surface charge prediction of our proposed model and the independent surface charge measurements of Huertas et al. (1998). This agreement strengthens the proposed model.

6. SUMMARY AND CONCLUSIONS

Steady-state kaolinite dissolution rates were examined using non-mixed flow-through reactors. The experiments were conducted at 25°C, 50°C and 70°C in a pH range of 0.5 to 4.5 at far-from equilibrium conditions ($-5.6 < \Delta G_r < -39$ kcal mol^{-1}). It was found that kaolinite dissolution rate increases with temperature and decreases with pH.

The results of the present study are insufficient to construct a full rate law of kaolinite dissolution under acidic conditions. However, they indicate that (in the absence of catalysts) the rate of kaolinite dissolution at pH range of 0.5 to 4.5 is controlled by two independent parallel reaction paths. Each reaction path consists of fast adsorption of a proton on a different surface site followed by a slow hydrolysis step. We do not have any information regarding the identity of these active sites. Our proposed mechanism is similar to that proposed by Huertas et al. (1999) for the proton-promoted reaction of kaolinite at 25°C. In their model, Huertas et al. (1999) suggested that the two active sites that control the rate under acidic conditions are the edge and basal Al sites. The results of the present study neither support nor contradict this suggestion.

The first reaction mechanism controls the overall dissolution rate at pH $\geq$ 2.5, whereas the second mechanism controls it below pH 0.5. Between pH 0.5 and 2.5 both reaction paths influence the rate.

The results of the proposed model show that by proper separation of variables, the kaolinite dissolution rate may be described by a rate law using activation energies that are independent of pH. The apparent pH dependencies of the activation energies obtained by Carroll and Walther (1990) is a result of including the adsorption enthalpy term, which depends on the pH, in the activation energy term, as was also argued by Casey and Sposito (1992).

Acknowledgments—This research was supported by grant # ES-66-96 from the Israeli Ministry of Energy and Infrastructure and by the Belfer Foundation for Energy and Environmental Research. We wish to express our gratitude to J. Huertas and P. Brady for fruitful discussions and to E. Shani, A. Avital, R. Holzmann, N. Leshem, E. Roueff, G. Ronen O. Halabi and B. Kfir for their technical assistance. We thank the associate editor, Eric H. Oelkers, and J. Walther and two other anonymous reviewers for their review of the manuscript.

Associate editor: E. H. Oelkers

REFERENCES

Barrante J. R. (1974) Applied Mathematics for Physical Chemistry. Prentice-Hall, Inc.

Cama J., Ayora C., and Lasaga A. C. (1999) The deviation-from-equilibrium effect on dissolution rate and on apparent variations in activation energy. *Geochim. Cosmochim. Acta* **63(17),** 2481–2486.

Carroll S. A. and Walther J. V. (1990) Kaolinite dissolution at 25°, 60°, and 80°C. *Am. J. Sci.* **290,** 797–810.

Carroll-Webb S. A. and Walther J. V. (1988) A surface complex reaction model for the pH-dependence of corundum and kaolinite dissolution rates. *Geochim. Cosmochim. Acta* **52,** 2609–2623.

Casey W. H. and Sposito G. (1992) On the temperature dependence of mineral dissolution rates. *Geochim. Cosmochim. Acta* **56,** 3825–3830.

Devidal J.-L., Schott J., and Dandurand J.-L. (1997) An experimental study of kaolinite dissolution and precipitation kinetics as a function of chemical affinity and solution composition at 150°C, 40 bars, and pH 2, 6.8, and 7.8. *Geochim. Cosmochim. Acta* **61(24),** 5165–5186.

Dougan W. K. and Wilson A. L. (1974) The absorptiometric determination of aluminum in water. A comparison of some chromogenic reagents and the development of an improved method. *Analyst* **99,** 413–430.

Ganor J., Cama J., and Metz V. (2002) Coherency of surface protonation data: Implication from modelling of dissolution experiments. *Geochim. Cosmochim. Acta* **66**S1, A261 (abstr.).

Ganor J. and Lasaga A. C. (1998) Simple mechanistic models for inhibition of a dissolution reaction. *Geochim. Cosmochim. Acta* **62(8),** 1295–1306.

Ganor J., Metz V. (2001). To stir or not to stir - implications for silicate dissolution experiments. *Proceedings of 10th International Symposium on Water-Rock Interaction WRI-10* (ed. R. Cidu) **VI,** 271–274.

Ganor J., Mogollon J. L., and Lasaga A. C. (1995) The effect of pH on kaolinite dissolution rates and on activation energy. *Geochim. Cosmochim. Acta* **59,** 1037–1052.

Gautier J.-M., Oelkers E. H., and Schott J. (2001) Are quartz dissolution rates proportional to B.E.T. surface areas? *Geochimica. Cosmochimica. Acta* **65,** 1059–1070.

Huertas J. F., Chou L., and Wollast R. (1998) Mechanism of kaolinite dissolution at room temperature and pressure: Part 1. Surface speciation. *Geochim. Cosmochim. Acta* **62(3),** 417–431.

Huertas J. F., Chou L., and Wollast R. (1999) Mechanism of kaolinite dissolution at room temperature and pressure. Part II: Kinetic study. *Geochim. Cosmochim. Acta* **63,** 3261–3275.

Koroleff F. (1976) Determination of silicon. In *Methods of Seawater Analysis* (ed. K. Grasshoff)149–158. Verlag Chemie.

Lasaga A. C. (1981) Rate laws of chemical reactions. In *Kinetics of Geochemical Processes*, (eds. A. C. Lasaga and J. R. Kirkpatrick) Vol. 8, pp. 1–68. Mineralogical Society of America.

Metz V. and Ganor J. (2001) Stirring Effect on Kaolinite Dissolution Rate. *Geochim. Cosmochim. Acta* **65(20),** 3475–3490.

Mogollon J. L., Ganor J., Soler J. M., and Lasaga A. C. (1996) Column experiments and the full dissolution rate law of gibbsite. *Am. J. Sci.* **296,** 729–765.

Nagy K. L., Blum A. E., and Lasaga A. C. (1991) Dissolution and precipitation kinetics of kaolinite at 80°C and pH 3: The dependence on solution saturation state. *Am. J. Sci.* **291,** 649–686.

Nagy K. L. and Lasaga A. C. (1992) Dissolution and precipitation kinetics of gibbsite at 80°C and pH 3: The dependence on solution saturation state. *Geochim. Cosmochim. Acta* **56,** 3093–3111.

Oelkers E. H., Schott J., and Devidal J.-L. (1994) The effect of aluminum, pH, and chemical affinity on the rates of aluminosilicate dissolution reactions. *Geochim. Cosmochim. Acta* **58**(9), 2011–2024.

Palmer D. A. and Wesolowski D. J. (1992) Aluminium speciation and equilibria in aqueous solution: II. The solubility of gibbsite in acidic sodium chloride solution from 30 to 70°C. *Geochim. Cosmochim. Acta* **56,** 0001–0019.

Robie R. A., Hemingway B. S., Fisher J. R. (1978) Thermodynamic properties of minerals & related substances at 298.15K and 1 Bar (105 Pascals) pressure and at higher temperatures. In *U. S. Geological Survey Bulletin,* **Vol. 1452,** United States Government Printing Office.

Sverjensky D. A. and Sahai N. (1998) Theoretical prediction of single-site enthalpies of surface protonation for oxides and silicates in water. *Geochim. Cosmochim. Acta* **62(23/24),** 3703–3716.

Walther J. V. (1996) Relation between rates of aluminosilicate mineral dissolution, pH, temperature, and surface charge. *Am. J. Sci.* **296,** 693–728.

Wieland E. and Stumm W. (1992) Dissolution kinetics of kaolinite in acidic aqueous solutions at 25°C. *Geochim. Cosmochim. Acta* **56,** 3339–3355.

Wolery T. J. (1992) EQ3NR, a computer program for geochemical aqueous speciation-solubility calculations: theoretical manual, User's Guide, and related documentation (version 7.0), Lawrence Livermore National Lab, Berkeley, CA.